Reactions and Thermochemistry of Alkyl Ions, $C_n H_{2n+1}+$ (n=1-8), in the Gas Phase

Skip Williams, Thomas M. Miller, W.B. Knighton, Anthony J. Midey, Susan T. Arnold, and A. A. Viggiano

Air Force Research Laboratories, Space Vehicles Directorate

Space Vehicles Directorate, 29 Randolph Road, Hanscom AFB, MA 01731-3010

Campbell D. Carter

Air Force Research Laboratories, Propulsion Directorate

Aerospace Propulsion Directorate, 1950 Fifth St., Wright-Patterson AFB OH 45433-7521

Abstract

Our research program focuses on identifying reaction processes important for plasma enhancement of combustion systems. Recommendations for temperature and energy dependencies of key ion-molecule reactions are made based on the laboratory measurements described above. Thermodynamic data such as heat capacity, entropy, and enthalpy are not available as a function of temperature for many of the ionic species formed in these reactions and are thus calculated using quantum mechanical methods. The resulting kinetic and thermodynamic data are being used to develop detailed kinetic mechanisms for incorporation into CFD models. In the present contribution, reaction rate measurements and thermochemical computations pertaining to alkyl ions, CnH2n+1 + (n=1-8) are incorporated into a detailed combustion mechanism, and calculations of the ignition delay time are performed. The result of the ignition delay time for an isooctane/O2/Ar/NO mixture to be used in shock tube ignition studies is presented.

Introduction

The development of future aerospace vehicles requires a precise understanding of the associated fluid dynamics and chemistry-flowfield coupling. Furthermore, proposed magneto gas dynamic (MGD) applications require a detailed understanding of the plasma-chemistry-flow field coupling. While many aspects of plasma and combustion chemistry are known, the coupling of these two areas is not well characterized. This paper describes an experimental and theoretical computation program aimed at developing a better understanding of the important and relevant ion chemistry in these plasma enhanced combustion environments.

Mixing and ignition are of fundamental interest in combustion and propulsion research. It is a general assumption that for similar conditions the better (faster) the mixing and ignition the

Report Documentation Page

Form Approved
OMB No. 0704-0188

1. REPORT DATE	2. REPORT TYPE	3. DATES COVERED
20 OCT 2003	**N/A**	**-**

4. TITLE AND SUBTITLE	5a. CONTRACT NUMBER
Reactions and Thermochemistry of Alkyl Ions, Cn H2n+1+ (n=1-8), in the Gas Phase	5b. GRANT NUMBER
	5c. PROGRAM ELEMENT NUMBER
6. AUTHOR(S)	5d. PROJECT NUMBER
	5e. TASK NUMBER
	5f. WORK UNIT NUMBER
7. PERFORMING ORGANIZATION NAME(S) AND ADDRESS(ES) **Air Force Research Laboratories, Space Vehicles Directorate Space Vehicles Directorate, 29 Randolph Road, Hanscom AFB, MA 01731-3010; Air Force Research Laboratories, Propulsion Directorate Aerospace Propulsion Directorate, 1950 Fifth St., Wright-Patterson AFB OH 45433-7521**	8. PERFORMING ORGANIZATION REPORT NUMBER
9. SPONSORING/MONITORING AGENCY NAME(S) AND ADDRESS(ES)	10. SPONSOR/MONITOR'S ACRONYM(S)
	11. SPONSOR/MONITOR'S REPORT NUMBER(S)

12. DISTRIBUTION/AVAILABILITY STATEMENT
Approved for public release, distribution unlimited

13. SUPPLEMENTARY NOTES
See also ADM001739, Thermochemical processes in plasma aerodynamics (Conference Proceedings, 28-31 July 20030 CSP 03-5031)., The original document contains color images.

14. ABSTRACT

15. SUBJECT TERMS

16. SECURITY CLASSIFICATION OF:			17. LIMITATION OF ABSTRACT	18. NUMBER OF PAGES	19a. NAME OF RESPONSIBLE PERSON
a. REPORT	b. ABSTRACT	c. THIS PAGE			
unclassified	**unclassified**	**unclassified**	**UU**	**25**	

Standard Form 298 (Rev. 8-98)
Prescribed by ANSI Std Z39-18

better the combustion efficiency. Previous efforts have established the effectiveness of utilizing high-temperature plasma jets to cause ignition and rapid flame propagation in hydrocarbon-air mixtures.[1,2] Renewed interest in the development of high-speed airbreathing propulsion technology has prompted a number of investigators to consider adopting plasmas as ignition aids in scramjet combustors with positive results. However, computational studies attempting to assess the importance of ion chemistry in combustion have been impeded by a lack of kinetic data at relevant temperatures.[3] Ionization and recombination processes at high temperatures have been studied in flames and shock tubes dating back many years.[4,5] However, the study of individual ion-molecule reactions under controlled conditions has been studied mainly at or near room temperature.[6] To date, numerous air plasma ion reactions with hydrocarbons at high temperature have been investigated in our laboratory, and these data are being compiled for use in computational modeling studies regarding the effects of ionization in combustion. Reactions of various atmospheric plasma ions (NO^+, N_2^+, O_2^+, O^+, N^+, H_3O^+) with aliphatic[7-9] and aromatic hydrocarbons[10-12] have been studied as a function of temperature using flow-tube methods. Incorporating these ionic reactions into detailed neutral hydrocarbon combustion kinetics models demonstrates that ionization speeds the rate of combustion.[13,14] The detailed neutral mechanism used previously at AFRL is based on the validated[15] n-heptane mechanism developed by Lindstedt and coworkers[16-18] with the addition of several reactions pertaining to the combustion of branched alkanes to model isooctane combustion. Measurements of the spontaneous ignition of isooctane obtained in a rapid compression machine[19] at a pressure of ca. 10 atm over the 900-950K temperature range have been well described using the modified n-heptane C/H/N/O mechanism. The CONP program of the CHEMKIN II software series[20] was used for the computations**.** There is excellent agreement between the calculated ignition delay time and the experimentally observed values as a function of the compressed gas temperature, taken as the initial temperature in the computations.[21]

Our first studies focused on evaluating whether introducing weakly ionized air into a ramjet/scramjet combustor would significantly improve hydrocarbon combustion.[21,22] Some interesting conclusions of this work are that the residual ionization levels entering the combustor from any preionization of air exterior to the vehicle would not be sufficient to significantly affect combustion, i.e., the ionization levels would be reduced to sub part-per-million levels due to recombination before reaching the combustor. These calculations further suggest that a plasma source must be present internal to the combustor to produce the ionization levels necessary to significantly reduce the ignition delay time. This conclusion is being evaluated in test conducted at the continuous flow scramjet facility at AFRL/PR at WPAFB [23,24] where plasma sources are being developed for use inside the combustor for ignition.

Placing a plasma source inside a supersonic combustor results in a new and significantly more difficult modeling problem, because generating the plasma in a hydrocarbon environment greatly increases the number and types of reactions that need to be considered. Furthermore, models, which hope to accurately predict plasma gas dynamic effects in the combustor, must include hydrocarbon ion chemistry in order to be able to fully represent the ionization level of the gas. Knowledge of such reactions is crucial for mechanism development and can be a daunting task for jet fuels consisting of mainly C_8-C_{12} hydrocarbons, because the number of neutral reactions that must be included increases dramatically with increasing carbon number of the fuel. Luckily, only a relatively small number of secondary hydrocarbon ions have been encountered for the large number of ion-molecule reactions studied.[7-12,25] For example, for air plasma ions reacting with an alkane series given by the formula C_nH_{2n+2}, ions with the formula $C_mH_{2m+1}^+$ ($m \leq n$) are formed predominately. Specifically, for air plasma ions reacting with larger alkanes up to octane ($n>5$), $C_3H_7^+$, $C_4H_9^+$, $C_5H_{11}^+$, $C_6H_{13}^+$, $C_7H_{15}^+$, $C_8H_{17}^+$ ions are formed and account for a large fraction (ca. 65%) of the reactivity. Table 1 below shows the ionization energy of some simple hydrocarbon ions formed in these reactions compared with alkali ions and common air plasma ions. Values are taken from the NIST database.[26] The ionization energies of the hydrocarbon species are significantly lower than the air species and are almost as low as the alkali metals in some cases. Therefore, one may expect that these ions are going to be the positive charge carriers in large hydrocarbon combustion environments. Consequently, the ion-molecule and electron-molecule reactions that determine the life cycle of these ions will be an important consideration for any plasma-based applications. This statement follows from the fact that these ions may govern the electron lifetimes due to the large dissociative recombination rates observed for these ions.[27-31] In most cases the dissociative recombination rates of these ions is almost an order of magnitude larger than that for NO+ at combustion temperatures.

Table 1: Ionization energies (IE) in eV of some simple hydrocarbon species. The ionization energies of the air plasma and alkali species are shown for comparison.

Species	IE (eV)
N_2	15.6
CH_4	12.5
O_2	12.1
NO	9.26
C_2H_3	8.9
l-C_3H_3	8.7
i-C_3H_7	7.36
t-C_4H_9	6.70
C_5H_{11}	6.65
c-C_3H_3	6.6
Na	5.14

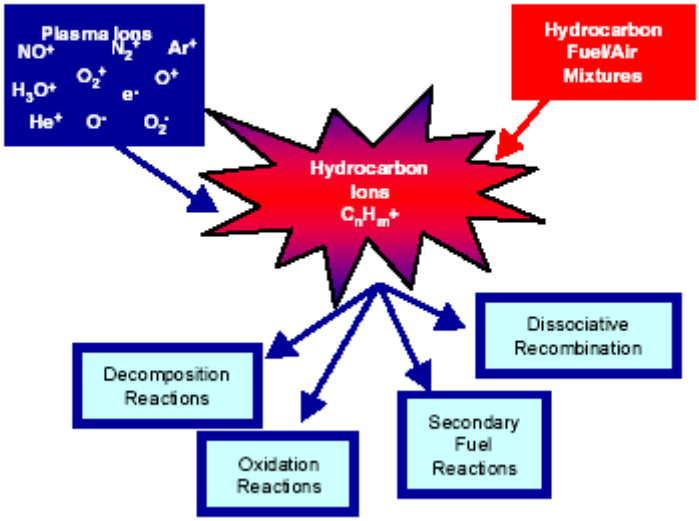

Figure 1: Reaction path block diagram illustrating the important ion processes important in a plasmaaugmented hydrocarbon combustor

Because air plasma ions are rapidly converted to more stable hydrocarbon ions in the combustor, it is necessary to include reactions of hydrocarbon ions with air components, fuel components, combustion byproducts, and electrons. A reaction path block diagram illustrating these points is shown in Figure 1. In particular, reactions are being studied with a variety of species including O2, O, O3, OH, H, alkanes, alkenes, alkynes, and aromatics in our laboratory and dissociative recombination reactions capable of identifying the neutral products are being conducted in collaboration with Larsson and coworkers at the ion storage ring in Stockholm. Selected important and interesting aspects of these unpublished, results are outlined below.

Secondary Hydrocarbon Ion Reactions

The plasma chemistry of ionized air reacting with hydrocarbons is investigated using fast ion flow tube kinetic instrumentation. The variable temperature-selected ion flow tube (VT-SIFT) instrument[32] can be used to measure both reaction rate constants and branching fractions as a function of temperature from 80 to 550 K. Measurements at higher temperatures are conducted using a second fast flow tube instrument, the high temperature flowing afterglow (HTFA) instrument.[33,34] The HTFA provides data from 300 to 1800 K enabling the study of ion-

molecule reactions at temperatures relevant to plasma and combustion chemistry. Both instruments operate at ca. 1 Torr helium buffer pressure, and the kinetics are observed over ca. 1-4 ms reaction time. Each apparatus has been discussed previously and the following discussion focuses on some recent results.

The oxidation of hydrocarbon ions in plasma augmented environments is of fundamental interest. Initial investigations involve hydrocarbon ions reacting with O_2, because O_2 and N_2 are the most likely collision partners early in the ignition process. Since N_2 is unreactive and O_2 is present initially in such a large concentration compared to the combustion byproducts, even limited reactivity with O_2 would be an important process. For example, the case of the tertiary butyl ion ($t\text{-}C_4H_9^+$) reacting with O_2,

$$t\text{-}C_4H_9^+ + O_2 \longrightarrow C_2H_5O^+ + C_2H_4O, \quad \Delta H = -299 \text{ kJ/mol} \quad (1a)$$
$$\longrightarrow C_2H_3O^+ + C_2H_6O, \quad \Delta H = -293 \text{ kJ/mol} \quad (1b)$$
$$\longrightarrow HCO^+ + C_3H_8O, \quad \Delta H = -158 \text{ kJ/mol} \quad (1c)$$
$$\longrightarrow C_2H_2O+ + C_2H_6O, \quad \Delta H = -67 \text{ kJ/mol} \quad (1d)$$

has several reaction channels that are exothermic by over 150 kJ/mol. However, the rate constant observed for this reaction is immeasurably small at 300 K with an upper limit of 10^{-13} cm^3-s^{-1}, which is the current detection limit of our apparatus. CH_3^+, $C_2H_5^+$, $i\text{-}C_3H_7^+$, $sec\text{-}C_4H_9^+$, $C_5H_{11}^+$, and $i\text{-}C_8H_{17}^+$ are also unreactive with O_2 at 300 K, $k < 5x10^{-13}$ cm^3 s^{-1}, despite the availability of reaction channels with exothermicities of several hundred kJ/mol.

The next step is to study the reactivity of these ions with other oxidizing agents such as O atoms. However, the quantification of O atoms as a reactant poses a problem making the experiments difficult. Oxidation reactions with ozone have been conducted in the meantime and have provided interesting results. Oxidation by ozone may provide insight into the O atom reactions because the small O_2-O bond energy. Furthermore, density functional calculations[35] indicate a mechanism involving initial complex formation of hydrocarbon cations with O_3, followed by O-O_2 cleavage, and finally hydrogen and alkane elimination to yield the highly exothermic products listed in Table 2. According to this mechanism, the O_3 and O atom reactions may share common intermediates and studying the O_3 oxidation may lead to some insight into the more difficult O atom studies.

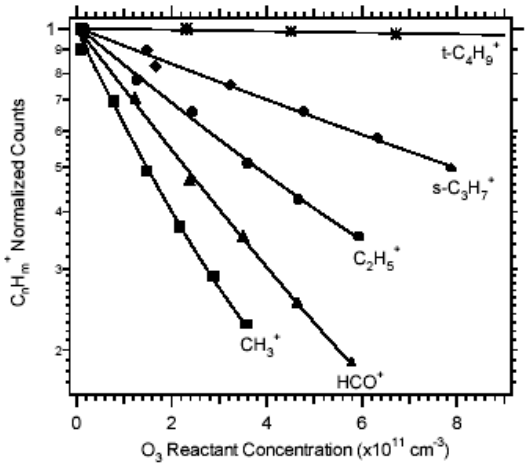

Figure 2: Primary ion decay plots for CH_3^+ (squares), HCO^+ (triangles), $C_2H_5^+$ (circles), s-$C_3H_7^+$ (diamonds), and t-$C_4H_9^+$ (asterisks) reacting with O_3. The solid lines are nonlinear least squares fits to the data performed to determine the rate constants. Experiments were performed with a reactant gas composition of 5% O_3 in O_2 which is possible since O_2 is unreactive.

Table 2: Reaction rate constants for reactions of ozone at 300 K measured with the selected ion flow tube (SIFT). The calculated collision rate constant, *kc*, and the measured rate constant, *k*, are listed in italics. The reaction products and branching fractions are listed under the rate constants. Energetics are taken from the NIST Chemistry WebBook.[36] Neutral products are not resolved in these experiments. Brackets indicate that more than one product channel could contribute to the branching fraction. Products contained in parentheses are estimated based on the mechanism discussed in the text involving O_2 loss. Note that the reactions are considerably more exothermic if the reaction products in parenthesis are not dissociated.

Reaction	Products	*k; [kc]* (10^{-9} cm^3 s^{-1})	Branching Fractions	ΔH, kJ/mol
$HCO^+ + O_3 \rightarrow$		*1.2;[1.3]*		
	$HO_3^+ + CO$		> 0.98	-31.5
$CH_3^+ + O_3 \rightarrow$		*1.7;[1.6]*		
	$HCO^+ + (H_2 + O_2)$		0.66	-410
	$H_2CO^+ + HO_2$		0.16	-293
	$H_2O_2^+ + HCO$		0.10	-311
	$O_2^+ + CH_3O$		0.07	-54

	$H_3O^+ + CO_2$		<0.01	-1038
$C_2H_5^+ + O_3 \rightarrow$		*0.59;[1.3]*		
	$HCO^+ + (CH_4 + O_2)$		0.70	-294
	$C_2H_3O^+ + (H_2 + O_2)$		0.30	-392
s-$C_3H_7^+ + O_3 \rightarrow$				
	$C_2H_3O^+ + (CH_4 + O_2)$	*0.22;[1.2]*	0.64	-363
	$HCO^+ + (C_2H_6 + O_2)$		0.16	-200
	$CH_3O^+ + C_2H_4 + O_2$	}	0.14	-186
	$+ CH_3COOH$			-670
	$C_3H_3O^+ + 2H_2O$		0.05	-674
	$C_3H_6O^+ + HO_2$		0.01	-167
s-$C_4H_9^+ + O_3 \rightarrow$		*0.08;[1.1]*		
	$HCO^+ + (C_3H_8 + O_2)$		Major (~0.40)	-188
	$C_2H_3O^+ + (C_2H_6 + O_2)$		Major (~0.35)	-339
	$C_2H_5O^+ + C_2H_4 + O_2$	}	Minor (~0.14)	-273
	$+ CH_3COOH$		Minor (~0.09)	-758
	$C_2H_2O^+ + C_2H_6 + O_2$	}		-113
	$+ HOC_2H_4OH$		Trace (<0.02)	-423
	$CH_3O^+, C_3H_3O^+, C_3H_5O^+$			
t-$C_4H_9^+ + O_3 \rightarrow$		*<0.005;[1.1]*		
	$C_2H_3O^+ + (C_2H_6 + O_2)$			-284
	$HCO^+ + (C_3H_8 + O_2)$			-133
t-$C_5H_{11}^+ + O_3 \rightarrow$		*<0.005;[1.1]*		
	$C_2H_5CO^+ + (C_2H_6 + O_2)$			-296
				-255
	$C_2H_3O^+ + (C_3H_8 + O_2)$			-112
	$HCO^+ + (C_4H_{10} + O_2)$			

All of the cations listed showed no reactivity, $k < 5 \times 10^{-13}$ cm^3 s^{-1}, with O_2.

The following results have been observed for reactions with O_3. The total reaction rate constants for the alkyl carbocations decrease dramatically as the order of the reactant carbocation increases as shown in Figure 2 and listed in Table 2. In Figure 2, the slope of the line is

proportional to the reaction rate constant in our experiments. The primary carbocations CH_3+ and $C_2H_5^+$ react at 100% and 46% of the collision rate given by the Su-Chesnavich equation, respectively. The secondary s-$C_3H_7^+$ and s-$C_4H_9^+$ carbocations reacted with O_3 at 19% and 7% of the collision rate, respectively. The tertiary carbocations t-$C_4H_9^+$ and t-$C_5H_{11}^+$ were found to be unreactive with O_3, $k < 5x10^{-12} cm^3\ s^{-1}$, which is the detection limit of our apparatus using this ozone source.

The HCO^+ cation is a major product of the primary and secondary carbocation reactions with O_3 listed in Table 2. HCO+ is known to be unreactive with O_2,[37] and that finding was confirmed in this study. The major product of HCO^+ reacting with O_3 is HO_3^+. The branching fraction reported in Table 2 is >0.98 and is intended to reflect the uncertainty of the source conditions. The measured rate constant of $1.2 \times 10^{-9}\ cm^3\ s^{-1}$ is nearly equal to the thermal capture rate constant of $1.3 \times 10^{-9}\ cm^3\ s^{-1}$.

The methyl cation was prepared by ionization of methyl bromide and was selectively injected into the flow tube. However, despite very low injection energies, approximately 12% of the CH_3^+ collisionally dissociated to form CH^+ and CH_2^+. While these breakup products do not interfere with the reaction rate constant determination, they do react with O_2 to form some of the same products observed in the $CH_3^+ + O_3$ reaction.[38] Namely, CH^+ and CH_2^+ react with O_2 with rate constants of $9.7x10^{-10}\ cm^3\ s^{-1}$ and $9.1x10^{-10}\ cm^3\ s^{-1}$, respectively, and produce the following products[38]

$$CH^+ + O_2 \rightarrow HCO^+ + O \text{ (major)}, \quad (2a)$$
$$\rightarrow O^+ + HCO \text{ (minor)}, \quad (2b)$$
$$\rightarrow CO^+ + OH \text{ (minor)}, \quad (2c)$$

and

$$CH_2^+ + O_2 \rightarrow HCO^+ + OH \text{ (major)}, \quad (3a)$$
$$\rightarrow H_2CO^+ + O \text{ (minor)}. \quad (3b)$$

The methyl cation, on the other hand, does not undergo two body reactions with O_2 and only exhibits a slow ternary association reaction $k_{300K} = 8.6x10^{-30}\ cm^6\ s^{-1}$.[38,39]

Therefore, the impurity CH^+ and CH_2^+ ions were eliminated before entering the reaction zone by adding a small amount (5 SCCM) of O_2 approximately 20 cm upstream of the first reactant inlet. The O^+ and CO^+ ion resulting from reactions are converted to O_2^+ via charge transfer with O_2, and the H_2CO^+ is converted to HCO^+ (major) and $H_2O_2^+$ (minor) via reaction with O_2. After the addition of O_2 at inlet 1, the resulting ion composition in the flow tube at the reactant inlet was observed to be approximately 88% CH_3^+, 8.5% HCO^+, 2.5% O_2^+ and ~1% $H_2O_2^+$. The O_2^+ and $H_2O_2^+$ ions were accounted for by subtracting their baseline intensities observed at zero O_2/O_3 reactant flow from the appropriate product ion intensities. The HCO^+ ion

counts observed at zero O_2/O_3 reactant flow were corrected for by subtracting the appropriate number of counts at each ozone concentration based on the reactivity of HCO^+ with O_3 listed in Table 2.

The methyl cation reacts at the collision rate with O_3 producing HCO^+ as a major product and H_2CO^+, $H_2O_2^+$, O_2^+, and H_3O^+ as minor products. The product ion counts observed for H_2CO^+, $H_2O_2^+$, and O_2^+ were significantly above the background counts discussed for these ions. Therefore these ions are confirmed products. The H_3O^+ product, on the other hand, either results from direct reaction of CH_3^+ with O_3, which is highly exothermic but involves significant rearrangement, or from secondary reactions of HCO^+ with the very low level of H_2O present in the flow tube. Secondary chemistry can be accounted for by extrapolating the baseline corrected product branching fraction back to zero reactant concentration.[40] However, this approach did not fully account for the amount of H_3O^+ observed. Therefore, H_3O^+ is listed as a trace product in the reaction of $CH_3^+ + O_3$.

The ethyl cation, prepared by ionizing ethyl bromide, reacts with O_3 to form two primary products HCO^+ and $C_2H_3O^+$. Because $C_2H_5^+$ and HCO^+ are mass coincident two separate experiments were performed to determine the reaction rate constant. One experiment involved the addition of CH_3Cl to flow tube via inlet 1. Methyl chloride reacts with HCO^+ by proton transfer to form CH_4Cl^+ and was not intended to react with $C_2H_5^+$. However, the addition of methyl chloride did cause a reduction in the $C_2H_5^+$ signal and produced several unidentified high mass ions containing chlorine so that the amount of methyl chloride added was such that only about 20% of the original $C_2H_5^+$signal remained. In a second experiment $^{13}CCH_5^+$ ion was injected into the flow tube. Statistically equal amounts of $^{12}CHO^+$ and $^{13}CHO^+$ are assumed to be formed, and the intensity of $^{12}CHO^+$ is used as a measure of the $^{13}CHO^+$ contribution to the m/z = 30 (sum of $^{13}CCH_5^+$ + $^{13}CHO^+$). The reaction rate constant was determined by subtracting the intensity monitored at m/z 29 (12-CHO^+) from m/z = 30 (sum of $^{13}CCH_5^+$ + $^{13}CHO^+$) and plotting the decay of resulting ion signal as a function of O_3 flow. The two different experiments produced the following results. Using the methyl chloride scavenger three determinations yielded $6.3x10^{-10}$, $6.5x10^{-10}$ and $5.7x10^{-10}$ cm^3 s^{-1}. The $^{13}CCH_5^+$ experiment in a single determination yielded 5.2 $x10^{-10}$ cm^3 s^{-1}. The reaction rate constant in the Table is the average of the four measurements.

The reaction product branching fraction was estimated by injecting ^{12}C form of $C_2H_5^+$ using high O_3 flows where no intensity at m/z = 29 remained, i.e., $C_2H_5^+$ totally reacted and all of the HCO^+ was converted to HO_3^+. Approximately 5% of the $C_2H_5^+$ dissociated to $C_2H_3^+$ upon injection into the flow tube. The reaction products originating from $C_2H_3^+$ were not identified or corrected for and constitute no more than a 5 percentage point uncertainty, i.e., the original

fraction of the $C_2H_3^+$ reactant ion intensity assuming it yields only a single product in the reported values. Since there are no minor channels, the presence of $C_2H_3^+$ has a small effect on the overall reported branching fractions.

The propyl radical cation was prepared by ionizing i-propyl bromide in the supersonic source. Approximately 5% of the $C_3H_7^+$ dissociated to $C_3H_5^+$ upon injection into the flow tube. Because $C_2H_3O^+$ is a major product of the sec-propyl cation reaction with O_3 and is mass coincident with $C_3H_7^+$, the reaction rate constant was determined by injecting the $^{13}CC_2H_7^+$ (m/z=44) form of the reactant ion. Given that the expected $C_2H_3O^+$ product distribution is 33% $C_2H_3O^+$ (m/z =43) and 67% $^{13}CCH_3O^+$ (m/z =44) then the $I(C_3H_7^+) = I(m/z=44) – 2*I(m/z =43)$. The reaction rate constant was determined using the corrected $C_3H_7^+$ intensity. The product branching fractions were determined from the same 13C experiments as follows: $I(C_2H_3O^+) =3*I(^{12}C_2H_3O^+)$, $I(HCO^+) = I(^{12}CHO^+) + I(^{13}CHO^+)$, $I(CH_3O^+) = I(^{12}CH_3O^+) + I(^{13}CH_3O^+)$ with the remaining C3 products exhibiting only a single peak. Three determinations were averaged and yielded 16% CHO^+, 14% CH_3O^+, 64% $C_2H_3O^+$, 5% $C_3H_3O^+$, and 1% $C_3H_6O^+$. The reaction products originating from $C_3H_5^+$ have not been positively identified but can be deduced to be either CHO^+ and/or $C_2H_3O^+$ based on the observed product distributions for the $C_3H_7^+$ and s-$C_4H_9^+$ (see below) reactant ions. Note that both $C_3H_7^+$ and s-C4H9+ show a small amount of dissociation to $C_3H_5^+$ upon injection into the flow tube and that only products common to both reaction systems can be possible reaction products of $C_3H_5^+$ and O_3. The influence of the $C_3H_5^+$ on the reported branching fractions has not been corrected for but constitutes no more than a 5 percentage point uncertainty (original fraction of the reactant ion intensity yielding a single product) in the reported values of the HCO^+ and $C_2H_3O^+$ product channels.

Previous theoretical studies at the Hartree-Fock and MP2 levels of theory on the character of the potential energy surface of the propyl cation[41] conclude that there exist two global minima, that for the secpropyl cation and that for corner-protonated cyclopropane. These calculations showed that a minimum does not exist that corresponds to the npropyl cation, which appears to be only a transition structure in the interconversion of the sec-propyl cation and the corner-protonated cyclopropane cation. According to these calculations, the n-propyl cation is 80.5 kJ/mol higher and the corner-protonated cyclopropane cation is 30 kJ/mol higher in energy than the sec-propyl cation structure. Furthermore, experimental investigations of the interconversion of the propyl cation structures demonstrate rapid rearrangement to the sec-propyl cation form. A detailed study by Ausloos and coworkers[42] showed that n-propyl cations isomerize intramolecularly to either isopropyl ions or protonated cyclopropane ions within 10^{-10} s. Rearrangement to the isopropyl ion is favored and increases in importance with increasing internal energy content of the ion. Mass spectrometric investigations suggest that the

isomerization of the corner-protonated cyclopropane structure to the isopropyl structure requires 10^{-7} to 10^{-5} s.[43,44] All of these isomerization times are much shorter than the approximately 1 ms it takes the ions to leave the source region and travel to the reactant inlet. Therefore, the reactivity shown in Table 2 for the propyl cation has been assigned to the s-$C_3H_7^+$ isomer.

To confirm this hypothesis, the propyl cation was also prepared by ionizing n-propyl bromide in the supersonic source. The kinetics measurements were performed using the $^{13}CC_2H_7^+$ ion and corrected for $^{13}CCH_3O^+$ product as described in the experiment using i-propyl bromide in the source. The product branching distribution was determined from the mass spectrum recorded with 100 SCCM of O_3 where no $C_3H_7^+$ remains. As above no correction for the products originating from $C_3H_5^+$ (~ 5% of the original reactant ion intensity) was made. The reaction rate constants and the product distributions for the $C_3H_7^+$ ions generated from n-propyl bromide is found to be nearly identical to that produced from i-propyl bromide. The minor differences observed in the branching ratios can be attributed to statistical deviations in the reproducibility of the measurements and small differences in the source and injection conditions. This result is consistent with the theoretical and experimental studies discussed above regarding the stability and isomerization processes of the $C_3H_7^+$ ions, which indicate that only the s- $C_3H_7^+$ isomeric form of the ion is present in our experiments.

In pulsed ion cyclotron resonance (ICR) experiments, Shold and Ausloos[45] observed that $C_4H_9^+$ cations formed by electron impact ionization of isobutane, neopentane, 2,2-dimethylbutane, i-butyl halides, and t-butyl halides all have the tertiary structure. Fragmentation of n-alkanes, 2-methylbutane, 3-methylpentane, n-butyl halides, and sec-butyl halides produce both s-$C_4H_9^+$ and t-$C_4H_9^+$ with the s-$C_4H_9^+$ surviving without rearrangement for at least 0.1 s. However, in the case of the halides, a collision-induced isomerization of the s-$C_4H_9^+$ to the t-$C_4H_9^+$ was found to occur. The ICR experiments of Shold and Ausloos were conducted at pressures of ca. 10^{-6} Torr and observation times ranging from 10^{-3} to 0.5 s. The temperature in the analyzer cell was kept at 320 K and the electron energy was varied between 10 and 25 eV. [45]

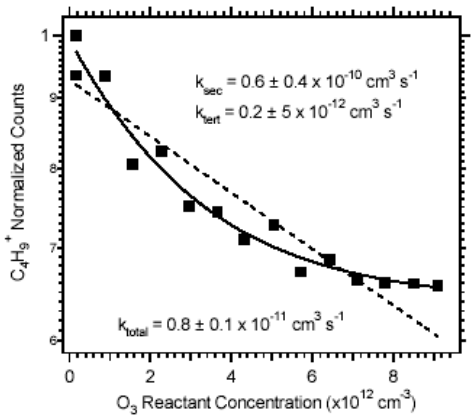

Figure 3: Normalized $C_4H_9^+$ counts (squares) plotted vs. O_3 concentration. The dashed line is the result of a single exponential fit of the data to determine the rate constant according to Equation (3). The result of the single exponential fit is labeled k_{total}. The solid line is the result of a double exponential fit of the data which yields a fast component (k_{sec}) with a rate constant of 6 ± 4 x 10^{-11} cm^3 s^{-1} and a slow component (k_{tert}) with a rate constant < 5 x 10^{-12} cm^3 s^{-1}.

Based on the Shold Ausloos results, [45] the tertbutyl cation was prepared by electron impact ionization of tert-butyl chloride in the supersonic argon expansion. The reported reaction rate constant was measured by increasing the flow tube pressure to 0.64 Torr (throttling the roots pump) and provided a measured value of < 3.4x10^{-12} cm^3 s^{-1} which is at the detection limit of our experiments with O_3 as a reactant and therefore represents an upper limit. No reactivity of t-$C_4H_9^+$ with O_2 was observed either, i.e., k < 3 x10^{-13} cm^3 s^{-1}.

The sec-butyl cation was prepared by ionizing *n*butyl bromide in the supersonic source. Injection of $C_4H_9^+$ into the flow tube yielded approximately 93% $C_4H_9^+$, 5% $C_3H_5^+$ and 2% $C_2H_5^+$. The electron impact ionization of *n*-butyl bromide produces both s- $C_4H_9^+$ and t- $C_4H_9^+$ and collisions with halide molecules in the source region can convert s- $C_4H_9^+$ to t- $C_4H_9^+$.[45] The kinetics plots with the $C_4H_9^+$ cation exhibited curvature indicating the presence of more than one form of $C_4H_9^+$. Using a large number of flow points and fitting the data as a double exponential with a non-linear least squares analysis program provides an estimate of the relative amounts of the two types of $C_4H_9^+$ and a measure of the rate constant for the fast reacting species. Figure 3 shows the normalized counts of the $C_4H_9^+$ reactant ion plotted as a function of the ozone reactant concentration. The result of a single exponential fit to the data yielded the dashed line associated with the rate constant designated ktotal. The single exponential fit reproduces the data very poorly, however, a double exponential fit provides a much better representation of the data. Free fitting several sets of data for the two rate constants yields a fast component with a rate constant of 8 x 10^{-11} cm^3 s^{-1} and a slow component with a rate constant < 4 x 10^{-12} cm^3 s^{-1}. No reactivity of either form of $C_4H_9^+$ with O_2 was observed, i.e., k < 3x10^{-13} cm^3 s^{-1}. It is assumed that the slower reacting component is the tert-butyl cation (ca. 67%) and the faster reacting component is sec-butyl cation (ca. 33%).

Additional insight into the relative amounts of the different forms of $C_4H_9^+$ was obtained using 2-methylbutane as the neutral reactant in hydride transfer reactions as done by Shold and Ausloos[45] and Meot-Ner and Field.[46] The tertiary and secondary forms of $C_4H_9^+$ have markedly different rates for hydride transfer from 2-methylbutane (i- C_5H_{12}). Based on previous results,[6,46] the hydride-transfer rate constants for the following reactions

t- $C_4H_9^+$ + $(CH_3)_2CCH_2CH_3$ > i-C_4H_{10}, + t- $C_5H_{11}^+$,

k298 = 2x10-11 cm3 s-1 (4a)

and

s- $C_4H_9^+$ + $(CH_3)_2CCH_2CH_3$ > n- C_4H_{10} + t- $C_5H_{11}^+$,

$k298 = 4x10^{-10}$ cm^3 s^{-1} (4b)

differ by over an order of magnitude. Figure 4 shows a plot of the total $C_4H_9^+$ reaction ion concentration as a function of 2-methylbutane reactant concentration. A biexponential fit of the data plotted in Figure 4 yields two rate constants of 4.9 ± 1.9 x 10^{-10} cm^3 s^{-1} (35%) and 4.2 ± 1.4 x 10^{-11} cm^3 s^{-1} (65%). These hydride transfer rate constants are in good agreement with those reported previously, and this experiment confirms that approximately 35% of the ions formed under our conditions are s- $C_4H_9^+$

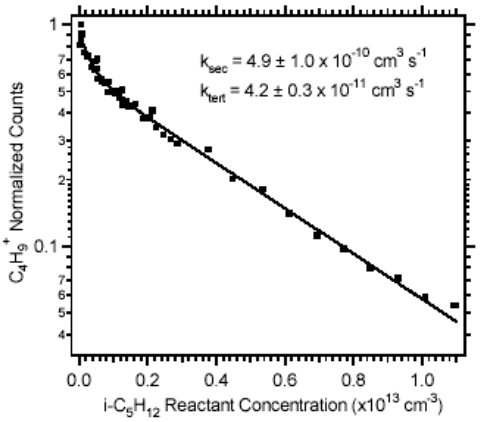

Figure 4: Normalized $C_4H_9^+$ counts (squares) plotted vs. 2-methylpentane (i-C_5H_{12}) concentration. The solid line is the result of a double exponential fit of the data which yields a fast component (k_{sec}) with a rate constant of 4.9 ± 1.0 x 10^{-10} cm^3 s^{-1} and a slow component (k_{tert}) with a rate constant 4.2 ± 0.3 x 10^{-11} cm^3 s^{-1}.

The product branching measurements are considerably more difficult than those of the reaction rate constant because most of the $C_4H_9^+$ is the nonreactive tertiary form. Hence the contribution of contaminant ions produced on breakup during injection, $C_2H_5^+$ and $C_3H_5^+$, are considerably larger compared to the products of the s-$C_4H_9^+$ primary ion. The major products observed are HCO^+ and $C_2H_3O^+$, and $C_2H_5O^+$ and $C_2H_2O^+$ are minor products. As shown in Table 2, reaction of $C_2H_5^+$ with O_3 produces HCO^+ and $C_2H_3O^+$, and $C_2H_5^+$ is unreactive with O_2. Since $C_2H_2O^+$ and $C_2H_5O^+$ were not observed in the experiments discussed above that contain the $C_3H_5^+$ impurity ion, these products most likely originate from the reaction of s-$C_4H_9^+$ with O_3. Given this level of uncertainty, the only conclusions that can be drawn are that HCO+ and $C_2H_3O^+$ are major products and that $C_2H_2O^+$ and $C_2H_5O^+$ are minor products produced in the reaction of s- $C_4H_9^+$ with O_3.

The production of $C_2H_5O^+$ in the reaction of s-$C_4H_9^+$ with O_3 is exothermic and is a conceivable product channel. The reaction for such a process is given below

s- $C_4H_9^+ + O_3 > C_3H_5O^+ + CH_4 + O_2$,

$$\Delta H = -393 \text{ kJ/mol.} \qquad (5)$$

Since $C_3H_5O^+$ is mass coincident with $C_4H_9^+$, the 13C $C_2H_5O^+$ (m/z=58) form of the reactant ion was injected into the flow tube. Assuming a statistical ^{13}C product distribution, approximately 25% of the $C_3H_5O^+$ product ion produced should be $C_3H_5O^+$ (m/z=57). Product branching fraction measurements taken at high resolution resulted in barely detectable amounts of $C_3H_3O^+$ (m/z=55), $^{13}C_3H_3O^+$ (m/z=56), and $C_3H_5O^+$ (m/z=57) are produced in the reaction. Trace amounts of ions at m/z=31 and m/z=32 were also observed and have been assigned to CH_3O^+ (m/z=31) and $^{13}CH_3O^+$ (m/z=32). Note that the CH_3O^+, $C_3H_3O^+$, and $C_3H_5O^+$ product ions could also originate from reaction of the $C_3H_5^+$ breakup ion (5%) reacting with O_3. Therefore, the CH_3O^+, $C_3H_3O^+$, and $C_3H_5O^+$ product ions are listed as trace product ions in Table 2.

The $C_5H_{11}^+$ radical cation was prepared by ionizing 2-chloro-2-methylbutane. The reported reaction rate constant for the $C_5H_{11}^+$ ion formed reacting with O_2 is $< 3x10^{-13}$ cm^3 s^{-1} and with O_3 is $< 4x10^{-12}$ cm^3 s^{-1}. The tertiary form of the $C_5H_{11}^+$ cation is the most stable form of this carbocation and electron impact ionization of the 2-chloro-2-methylbutane ion precursor is expected to produce this ion exclusively. The t- $C_5H_{11}^+$ cation is most stable cation studied in this series,[47] and, like the exceptionally stable t- $C_4H_9^+$ cation, it is not oxidized by either O_2 or O_3 even though several very exothermic products are available.

Thermochemical Calculations

Building a detailed kinetic mechanism requires an accurate knowledge of thermochemical data or reliable predictive models for such data. Calcote and Gill[48] have recently completed a comprehensive compilation of the heat of formation, entropy, and specific heat for ionic species as a function of temperature to 3000 K. Although this is one of the most complete compilations to date, many ions relevant to this work are not included. Furthermore, the thermodynamic properties of many of the ions that are included in the compilation are derived from group additivity methods or by comparisons to similar neutral species. Therefore, accurate thermodynamic data for an assortment of hydrocarbon intermediates important to developing mechanisms for plasma-enhanced combustion are still not available.

In order to address this important problem, *ab initio* quantum mechanical calculations[49] are being performed. These calculations allow the estimation of the heats and entropies of ionic species.[49] An example will be presented here. Density functional theory has been applied to elucidate the thermochemistry of propargyl radical (H_2C_3H) and cyclopropenyl radical (c-C_3H_3), for both neutrals and cations. The commonly used hybrid functional, Becke’s B3LYP, was utilized with a large basis set denoted by 6-311++G(3df,2p), which includes diffuse functions on

both the carbon and hydrogen atoms. The neutrals have doublet ground states, while the cations are both singlets. Both the neutral H_2C_3H and cationic $H_2C_3H^+$ are calculated to have C_{2v} symmetry. Neutral c- C_3H_3 is planar except for one H atom protruding out of plane; the point group is C_1. The c- $C_3H_3^+$ cation is planar (D_{3h} symmetry). The symmetry is important in determining entropy and free energy since the rotational symmetry numbers are different, from 1 for C_1 to 6 for D_{3h}. The ionization energy of H_2C_3H was found to be 8.72 eV, which may be compared to the NIST database value of 8.67 ± 0.02 eV. The heat of formation of $H_2C_3H^+$ was calculated by the atomization method and yielded Δ_fH_{ion} = 1192 kJ/mol, which may be compared with the NIST value of 1180 kJ/mol. For c- C_3H_3, the calculated IE is 6.18 eV, which may be compared to the NIST derived value of 6.6 eV. The calculated Δ_fH_{ion} (c-$C_4F_4^+$) is 1093 kJ/mol, which may be compared with the NIST value of 1080 kJ/mol. The differences in the calculated and experimental heats of formation are consistent with previous work, [50] but the discrepancy in the c- C_3H_3 IE is still under investigation.

For the combustion modeling described in this paper, the thermochemistry of the cations is needed. A harmonic approximation is used to obtain vibrational frequencies at the same level of theory as used for the structures and IEs, described above. The resulting frequencies were scaled by 0.989, recommended in the literature on the basis of comparison with experiment for a large number of molecules. Thermodynamic quantities calculated thusly compare well with JANAF values (0-2% up to 3000 K) for molecules with known thermochemistry. Error at high temperatures may be due to anharmonicity, which may eventually be corrected for in a semiempirical manner. The calculated heat capacities (C_p) of $H_2C_3H^+$ and c-$C_3H_3^+$ differ by 25% at 298 K, but at high temperatures become essentially indistinguishable, differing by less than 0.1% at 3000 K. The enthalpies likewise converge with temperature, albeit at higher temperatures. The entropies for these two isomers of $C_3H_3^+$ diverge with temperature because of the higher rotational symmetry number for c-$C_3H_3^+$, and thus the free energies also diverge, with those for c-$C_3H_3^+$ being higher.

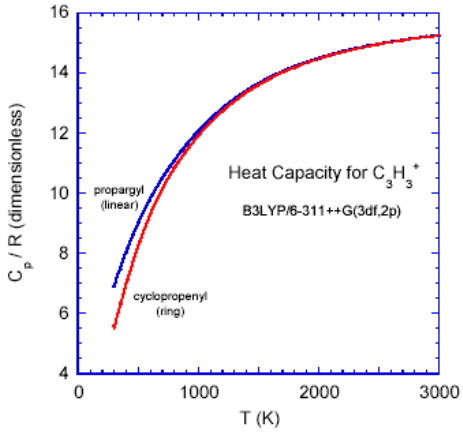

Figure 5a: Calculated heat capacities (C_p)

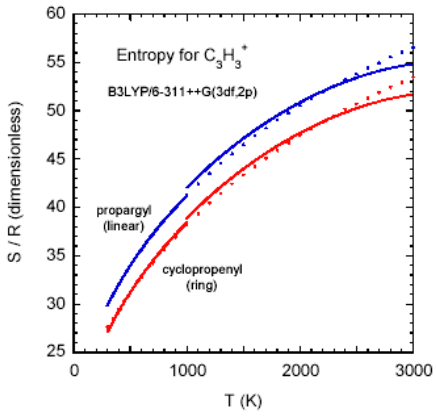

Figure 5b: Calculated standard

entropies (S_o) of $H_2C_3H^+$ and c- $C_3H_3^+$ as a function of temperature (dots) and fits to JANAF polynomials (lines).

of $H_2C_3H^+$ and c-$C_3H_3^+$ as a function of temperature (dots) and fits to JANAF polynomials (lines).

Table 3: Chemistry added to detailed C/H/N/O hydrocarbon/NO_x mechanism of Linstedt and Maurice.

Reactions Considered	Rate Coefficient			Comment
	$k = A\ T^b \exp(-Ea/RT)$			
	A	b	Ea	
	mole-cm^3-s^{-1}		J/mole	
Initiation				
$NO^+ + i\text{-}C_8H_{18} = HNO + i\text{-}C_8H_{17}^+$	1.14E+15	0.0	0.0	1
Thermal Decomposition				
$i\text{-}C_8H_{17}^+ = i\text{-}C_4H_8 + t\text{-}C_4H_9^+$ (high)	1.0E+9	0.0	35,000	2
$i\text{-}C_8H_{17}^+ = i\text{-}C_4H_8 + t\text{-}C_4H_9^+$ (low)	2.41E+15	0.0	35,000	2
Charge Transfer (Branching)				
$NO^+ + i\text{-}C_4H_8 = NO + C_4H_8^+$	1.02E+15	0.0	0.0	3
$NO^+ + i\text{-}C_4H_{10} = HNO + t\text{-}C_4H_9^+$	5.42E+14	0.0	0.0	1
Hydride Transfer (Fuel Breakdown)				
$t\text{-}C_4H_9^+ + i\text{-}C_8H_{18} = C_4H_{10} + C_8H_{17}^+$	2.40E+13	0.0	0.0	4
Dissociative Recombination				
$e^- + i\text{-}C_8H_{17}^+ = C_8H_{16} + H$ $= C_7H_{13} + CH_3 + H$	4.28E+18 4.28E+18	-0.5	0.0	5
$e^- + t\text{-}C_4H_9^+ = i\text{-}C_4H_8 + H$ $= C_3H_5 + CH_3 + H$	4.34E+18 4.34E+18	-0.5	0.0	5
$e^- + t\text{-}C_4H_8^+ = C_4H_7 + H$ $= C_3H_4 + CH_3 + H$	3.9E+18 3.9E+18	-0.5	0.0	6
Air Ionization				
$O + O + O_2 = O_2 + O_2$	9.79E+21	-2.0	0.0	7
$O + O + N_2 = O_2 + N_2$	1.21E+17	-1.0	0.0	7
$N + O_2 = NO + O$	6.44E+09	1.0	26,273.5	8
$O + N_2 = N + NO$	1.959E+14	0.0	321,102.0	8
$N + N + M = N_2 + M$	5.441E+17	-1.0	0.0	7
$N + O + M = NO + M$	7.254E+16	-0.5	0.0	7
$e^- + NO^+ = N + O$	1.70E+19	-0.7	0.0	7

1. Measured at AFRL references 7 and 9.

2. Estimated based on AFRL measurements.

3. Calculated based on AFRL measurements of similar systems.

4. Reference 6 and confirmed in AFRL measurements.

5. References 27-30. Rate coefficients are measured, but the products and temperature dependence are estimated.

6. Rate coefficients, products, and temperature dependence are estimated based on other measurements.

7. Reference 51.

8. Included in NO_x sub-mechanism of Maurice and coworkers and repeated here for completion.

Other ions under computational study include s-$C_3H_7^+$, t- $C_4H_9^+$, $C_6H_7^+$, i- $C_8H_{17}^+$, $C_8H_9^+$, $C_8H_{11}^+$ and $C_7H_7^+$ for which insufficient data as a function of temperature are available for detailed modeling applications. For the smaller molecules, application of Gaussian-3 (G3) theory is feasible, and should yield more accurate ionization energies (IE). G3 theory gives total energies which correspond effectively to calculations at the QCISD(T)/GTLarge level on MP2(full)/6-31G(d) optimized geometries, incorporating scaled HF/6-31G(d) zero-point energies and a "higher-level correction" term. Density functional theory (DFT) should give more accurate heat capacities and entropies because a much larger basis set is practical.

The G3 IE of iso- C_3H_7 was found to be 7.46 eV. If the G3 method is applied to the better DFT geometries of the neutral and cation, this result improves to 7.38 eV. The DFT value is 7.37 eV. These figures may be compared to the NIST database value of 7.37 ± 0.02 eV. These results are encouraging and suggest that IEs and thermochemical data can be successfully predicted within the DFT and G3 framework of model chemistries.

Kinetic Computations

In our previous paper, computations regarding the combustion of pure isooctane (i- C_8H_{18}), pure ethylbenzene (C_8H_{10}), and a 76 vol% isooctane / 24 vol% ethylbenzene mixture with a $H_3O^+/NO^+/e^-$ ionization kinetics scheme were discussed.[21] Isooctane and ethylbenzene were chosen because a mixture is a reasonable fuel ignition surrogate for JP-8 fuel. [22] Some of the key reactions included in modeling isooctane/ethylbenzene mixtures with a $H_3O^+/NO^+/e^-$ ionization scheme were also discussed. These detailed kinetic models — some having hundreds of elementary reaction steps — need validation. The companion paper **AIAA-2003-0703** describes the potential to use resonant enhanced multi-photon ionization (REMPI) to create a large initial concentration of NO^+ and low energy electrons within a shock tube. The goal of the experiment is to create a nearly instantaneous initial ionization condition to study of the effect of ions and low energy electrons on the ignition delay time of large hydrocarbon fuels. The experimental conditions of the shock tube measurements are an initial temperature of 1000 K and pressure of 1 atm. The gas composition in the measurements is 80% Ar, 17.6% O2, 1.4% isooctane, and 1% NO and the ionization is expected to produce ca. 1-5 x 10^{-4} mole fraction NO^+/e^- during the ca. 6 ns laser pulse duration.

Table 3 lists the ion-molecule processes that are considered for this experiment where i- and t- connote the iso- and tert- isomers, respectively, and the absence of a prefix indicates the normal isomer. The reaction set that needs to be considered in this experiment is relatively straightforward. NO^+ is unreactive with N_2, Ar, and O_2 and reacts at the collision rate with isooctane fuel.[6] Under our experimental conditions, dissociative recombination is competitive

with hydride transfer. At an intitial NO^+/e^- mole fraction of $1x10^{-4}$ ($8x10^{14}$ cm^{-3}) approximately 50% of the NO^+ ions undergo dissociative recombination and 50% undergo hydride transfer.

Isooctane reacting with NO^+ produces a large i- $C_8H_{17}^+$ ion which can recombine with electrons or undergo unimolecular dissociation at our temperatures. The primary product of the unimolecular dissociation is $C_4H_9^+$ and a tertiary structure is assumed here based on the precursor ion and the isomerization processes discussed in the experimental section. The unimolecular dissociation rate has been studied over the 300-500 K temperature range and only at ca. 0.4 Torr pressure. Meot-ner et al.[52] have studied the unimolecular decomposition of C_7 ions and found that at a few Torr pressure that the high-pressure limit had not been reached. A theoretical effort is underway to try to model this process. At present a Lindemann form for the pressure dependence that agrees with the available data is assumed and is listed in Table 3.

NO^+ is rapidly converted to i-$C_8H_{17}^+$ and t-$C_4H_9^+$ which then can react. However, as discussed in the experimental section, these ions are unreactive with Ar, N_2, and O_2. Furthermore, since both ions are tertiary ions, their oxidation reactions (if any) are expected to be too slow to compete with dissociative recombination and are not included. The next most important process is hydride transfer. Given the focus on ignition, hydride transfer reactions with the primary fuel have been considered. Furthermore, in the symmetric reaction of i- $C_8H_{17}^+$ with i- C_8H_{18}, the reactants are the same as the products, and it is not included. The t- $C_4H_9^+$ ion hydride transfer reaction rate constants are slow and decrease with increasing temperature.[46,53] A 300 K rate constant of 5×10^{-12} $(T/300)^{-4}$ cm^3 s^{-1} is used for the t- $C_4H_9^+$ ion reacting with i-C_8H_{18}. The rate constant at 300 K is measured,[54] and the temperature coefficient is taken from Meot-Ner et al. based on similar reactions with t-$C_4H_9^+$.[46,53]

The ion cycles shown in Table 3 are completed though neutralization reactions with thermal electrons. The NO^+ dissociative recombination reaction has been well studied as a function of energy and vibrational level. Many dissociative recombination rates for hydrocarbon ions have been measured by Mitchell and coworkers[27-30] and the available rates are included in Table 3. However, the branching fractions for these reactions are unknown. In our previous modeling, equal branching between the lowest energy dissociation channels, namely those leading to the production of –H atoms and -CH_3 radicals, was assumed. The ignition delay time for isooctane is a weak function of the relative fraction of each species, -H or -CH_3, produced in the dissociative recombination. This statement follows from our previous study where computations were performed involving selected atomic and radical species important in chain branching and propagation reactions. The ignition delay time of isooctane was reduced as the mole fraction of all chain branching and propagation species was increased. In general, O, H, OH, and CH_3 were found to be equally effective.

Even though the computations are relatively insensitive to the exact distribution of dissociative recombination products, they are sensitive to the total number of dissociation products. Specifically, if three body dissociation channels occur, especially those that produce two or more atomic or radical species, then the presence of these channels needs to be included. Recent results[55] conducted in collaboration with Larsson and coworkers at the ion storage ring in Stockholm demonstrate that for C_2 to C_3 containing hydrocarbon ions, several dissociation channels are produced with the majority being three-body channels. In light of these new results, the dissociative recombination channels for the i-$C_8H_{17}^+$ and t-$C_4H_9^+$ ions have been assigned 50% involving -H + -CH_3 production and 50% involving single -H atom production as shown in Table 3.

The reaction sequences shown in Table 3 describe the hydrocarbon ionization kinetics as well as the main air ionization and dissociation steps. These reactions have been added to the detailed hydrocarbon/NOx combustion mechanism of Lindstedt and coworkers.[16-18] In addition, a simple flame ionization mechanism of Pedersen and Brown[56] has also been added. Calculated thermochemical values discussed in the previous section are used where available. Both the detailed reaction mechanism and themochemical data are available upon request.

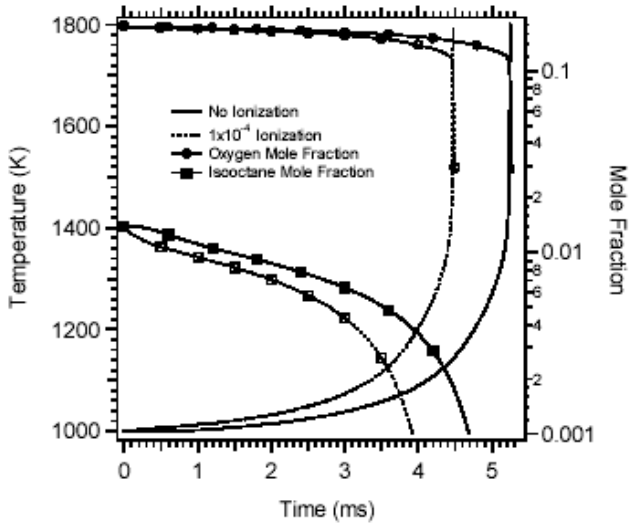

Figure 6. Species concentration and temperature as a function of time for 1.4% C_8H_{18}, 17.6% O_2, 1% NO, 80% Ar combustion (Ц=1) at a constant pressure of 1 atm, Tinitial=1000 K with (dashed lines) and without (solid lines) ionization.

Computations are performed for pure isooctane/dry air combustion with a NO^+/e^- ionization kinetics scheme. Presently, the CONP program of the CHEMKIN II software series20 is employed, which assumes a time-dependent constant pressure process**.** This approach, although simple, does allow realistic studies of the chemistry and the mechanisms for flame

initiation to be studied and compared to shock-tube validation experiment. The results of several CONP computations are discussed below.

Results of the computations at 1000 K for isooctane ignition with and without an initial mole fraction ($1x10^{-4}$) of NO^+/e^- are shown in Figure 6. Additional initial conditions include equivalence ratio of $\Phi = 1.0$ and initial pressure of P = 1 atm. The ignition delay time, τ_{ig}, is defined as the time at which the gas reaches a temperature 500 K above the initial value, $T_{initial}$, and is easily seen in the figure as a nearly instantaneous increase in temperature on the millisecond time scale.

A 15% reduction in the flame induction time is seen in Figure 6 for an ionization fraction of 10^{-4} relative to the case of no ionization for this example. Larger reductions occur at lower temperatures, higher mole fractions, and leaner fuel mixtures.[13,21,22] The ion-molecule chemistry important for promoting ignition occurs on a very rapid timescale (10^{-8} s) compared to ignition (10^{-3} s) as shown in Figure 7a. The i- C_8H_{18} mole fraction is essentially constant on the 10^{-8} s time scale, validating the earlier assumption that ion reactions with combustion byproducts can be neglected.

In Figure 7a, the NO^+ mole fraction decreases rapidly due to dissociative recombination and hydride transfer with i- C_8H_{18}. Accordingly, an increase in the i- $C_8H_{18}^+$ concentration is observed. However, as i- $C_8H_{18}^+$ is being produced, it is rapidly consumed through dissociative recombination and unimolecular decomposition to produce t- $C_4H_9^+$. The t- $C_4H_9^+$ ion is very stable and generally unreactive. Within 10^{-7} seconds, t- $C_4H_9^+$ becomes the major positive charge carrier and is eventually consumed through dissociative recombination. The ion mole fraction decreases nearly by 3 orders of magnitude within 10^{-6} seconds resulting in the concomitant production of N, O, H, and CH_3 (Figure 7b) from the dissociation recombination reactions discussed above. No such fast processes are present in the thermal ignition mechanism as can be seen in Figure 7c where the O, H, CH_3, N (below scale) and ion/electron (below scale) mole fractions are orders of magnitude lower on the same time scale. Furthermore, neither the chemi-ionization mechanism involving the reaction of CH with O nor the thermal air ionization mechanism are active under these conditions on these time scales.

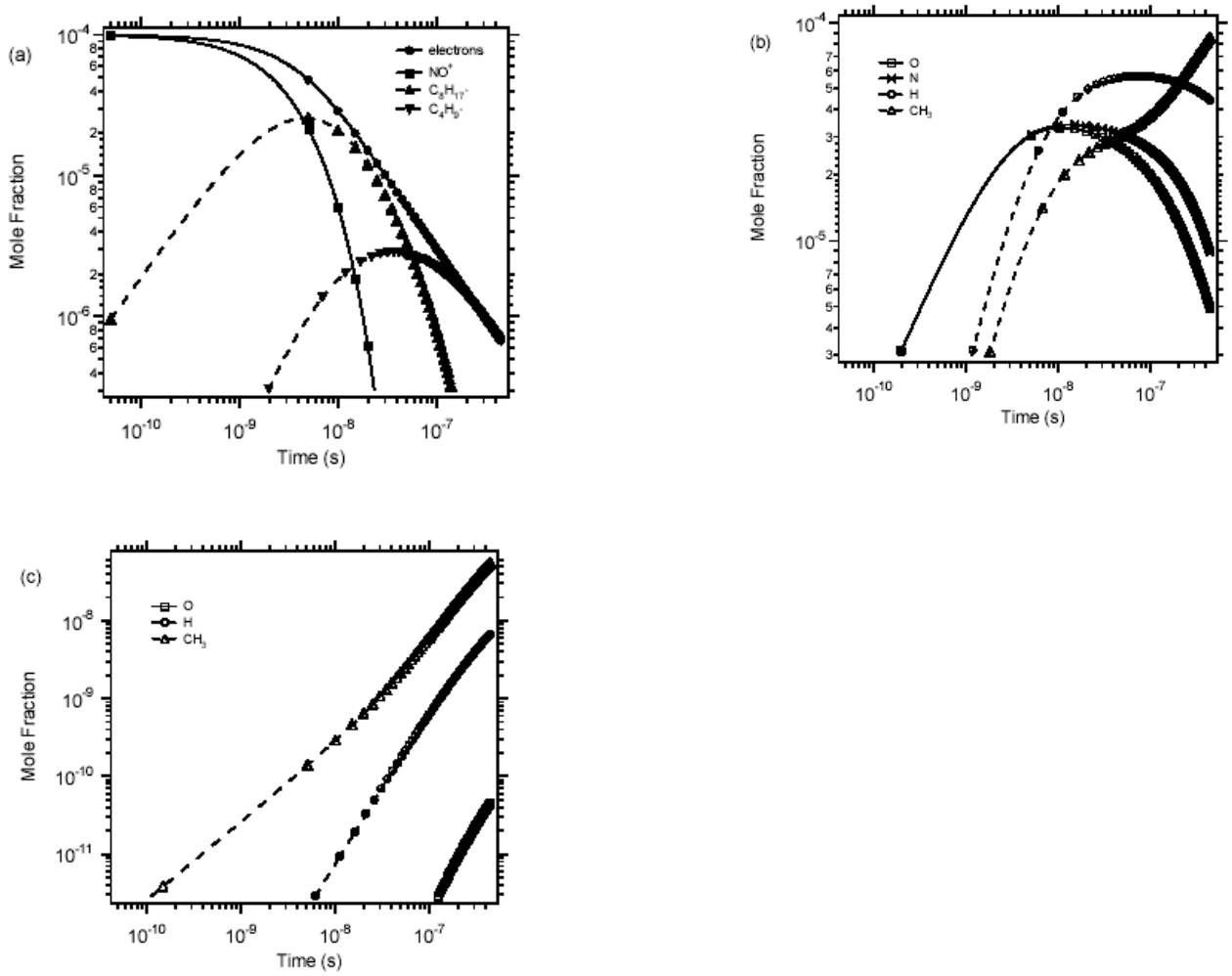

Figure 7. Same conditions as in Figure 6. (a) Major charged species profiles with ionization, (b) Major atomic and radical species profiles with ionization, (c) Major atomic and radical species profiles without ionization.

Conclusions

The flow tube kinetics measurements demonstrate that ions found in air plasmas do indeed react rapidly with aliphatic fuel constituents, leading to rapid decomposition of the alkane molecule and releasing reactive radicals. These reactions are typically much faster than the reactions between neutral species involved in hydrocarbon combustion initiation. Hydrocarbon bond cleavage, with the associated radical formation, is the crucial first step in hydrocarbon combustion. Combustion is generally initiated through either thermal decomposition of the fuel or relatively slow reaction between stable neutral species. The shock-tube measurements discussed in the companion paper **AIAA-2003-0703** will provide important validation data to substantiate these findings.

Models for plasma-based ignition, piloting, and combustion enhancement are useful toward guiding scramjet combustor design and development efforts. Techniques for improving

hydrocarbon fuel ignition characteristics have been shown to be enabling for viable hypersonic vehicles powered by scramjets. The efforts described in this contribution will be useful toward the design of efficient combustors for hypersonic propulsion systems. Moreover, the model development effort will facilitate our understanding of the detailed chemistry involved in these evolving technologies. Finally, since the methods being pursued are based on detailed fundamental kinetics treatments, the models developed within this program are broadly applicable to a range of diverse problems such as combustors for gas turbine engines, diesel engines, environmentally clean combustion, spark inhibition, and explosion limits in blended fuels.

Acknowledgements

The technical support of P. Mundis and J. Williamson is gratefully acknowledged. The financial support of the Air Force Office of Scientific Research (AFOSR) and the Nunn Program Office are gratefully acknowledged.

References

(1) Weinberg, F. J.; Horn, K.; Oppenheim, A. K. *Nature* **1978**, *271*, 341.

(2) Orrin, J. E.; Vince, I. M.; Weinberg, F. J. In *Eighteenth Symposium (International) on Combustion*; The Combustion Institute, 1981; pp 1755.

(3) Calcote, H. F.; Gill, R. J. Comparison of the Ionic Mechanism of Soot Formation with a Free Radical Mechanism; Bockhorn, H., Ed.; Springer-Verlag: Heidelberg, 1994; pp 471.

(4) *Ionization in High-Temperature Gases*; Shuler, K. E.; Fenn, J. B., Eds.; Academic Press: New York, 1962; Vol. 12.

(5) *Advanced Combustion Methods*; Weinberg, F.J., Ed.; Academic Press: London, 1986.

(6) Ikezoe, Y.; Matsuoka, S.; Takebe, M.; Viggiano, A. A. *Gas Phase Ion-Molecule Reaction Rate Constants Through 1986*; Maruzen Company, Ltd.: Tokyo, 1987.

(7) Arnold, S. T.; Viggiano, A. A.; Morris, R. A. *J. Phys. Chem. A* **1997**, *101*, 9351-9358.

(8) Arnold, S. T.; Morris, R. A.; Viggiano, A. A. *J. Phys. Chem. A* **1998**, *102*, 1345-1348.

(9) Arnold, S. T.; Viggiano, A. A.; Morris, R. A. *J. Phys. Chem. A* **1998**, *102*, 8881.

(10) Arnold, S. T.; Williams, S.; Dotan, I.; Midey, A. J.; Morris, R. A.; Viggiano, A. A. *J. Phys. Chem. A* **1999**, *103*, 8421.

(11) Midey, A. J.; Williams, S.; Arnold, S. T.; Dotan, I.; Morris, R. A.; Viggiano, A. A. *Int. J. Mass Spectrom.* **2000**, *195*, 327.

(12) Arnold, S. T.; Dotan, I.; Williams, S.; Viggiano, A. A.; Morris, R. A. *J. Phys. Chem. A* **2000**, *104*, 928-934.

(13) Williams, S.; Arnold, S. T.; Bench, P. M.; Viggiano, A. A.; Dotan, I.; Midey, A. J.; Morris, T.; Morris, R. A.; Maurice, L. Q.; Sutton, E. A. "Potential Enhancement of Hydrocarbon Fueled Combustor Performance via Ionization"; **ISABE 99-7236**, 14th International Symposium on Air Breathing Engines, 1999, Florence, Italy.

(14) Williams, S.; Midey, A. J.; Arnold, S. T.; Bench, P. M.; Viggiano, A. A.; Morris, R. A.; Maurice, L. Q.; Carter, C. D. "Progress on the Investigation of the Effects of Ionization on Hydrocarbon/Air Combustion Chemistry"; **AIAA 99-4907**, 9th International Space Planes and Hypersonic Systems and Technologies Conference, 1999, Norfolk, VA.

(15) Davidson, D. F.; Horning, D. C.; Hanson, R.K. "Shock Tube Ignition Time Measurements for n-Heptane/O2/Ar and JP-10/O2/Ar Mixtures"; **AIAA 99-2216**, 1999.

(16) Lindstedt, R. P.; Maurice, L. Q. *Combust. Sci. and Technol.* **1995**, *107*, 317-353.

(17) Lindstedt, R. P.; Maurice, L. Q. *Combust. Sci. and Technol.* **1996**, *120*, 119.

(18) Maurice, L. Q. Detailed Chemical Kinetic Models for Aviation Fuels. Ph.D. Thesis, Unversity of London, 1996.

(19) Griffiths, J. F.; Halford-Maw, P. A.; Mohamed, C. *Combust. Flame* **1997**, *111*, 327-337.

(20) Kee, R. J.; Rupley, F. M.; Miller, J. A., CHEMKIN II: A Fortran Chemical Kinetics Package for the Analysis of Gas Phase Chemical Kinetics; Sandia National Laboratories: Livermore, CA, April 1992.

(21) Williams, S.; Midey, A. J.; Arnold, S. T.; Miller, T. M.; Bench, P. M.; Dressler, R. A.; Chiu, Y.-H.; Levandier, D. J.; Viggiano, A. A.; Morris, R. A.; Berman, M. R.; Maurice, L. Q.; Carter, C. D. "Progress on the investigation of the effects of ionization on hydrocarbon/air combustion chemistry: kinetics and thermodynamics of C6-C10 hydrocarbon ions"; **AIAA 2001-2873**, AIAA 4th Weakly Ionized Gases Workshop, 2001, Anaheim, California.

(22) Williams, S.; Bench, P. M.; Midey, A. J.; Arnold, S. T.; Viggiano, A. A.; Morris, R. A.; Maurice, L. Q.; Carter, C. D., Detailed Ion Kinetic Mechanisms for Hydrocarbon/Air Combustion Chemistry. In *JANNAF Publication No. 703 entitled 37th Combustion, 25th Airbreathing Propulsion, 1st Modeling and Simulation Subcommittees* Monterey, CA, 2000; Vol. 1; pp 205-213.

(23) Mathur, T.; Streby, G.; Gruber, M.; Jackson, K.; Donbar, J.; Donaldson, W.; Jackson, T.; Smith, C.; Billig, F. "Supersonic Combustion Experiments with a Cavity-Based Fuel Injector"; **AIAA 99-2102**, 35th AIAA/ASME/SAE/ASEE Joint Propulsion Conference and Exhibit, 1999, Los Angeles, CA.

(24) Gruber, M. R.; Baurle, R. A.; Mathur, T.; Hsu, K.-Y. "Fundamental Studies of Cavity-Based Flameholder Concepts for Supersonic Combustors"; **AIAA 99-2248**, 35th AIAA/ASME/SAE/ASEE Joint Propulsion Conference and Exhibit, 1999, Los Angeles, CA.

(25) Williams, S.; Midey, A. J.; Arnold, S. T.; Morris, R. A.; Viggiano, A. A.; Chiu, Y.-H.; Levandier, D. J.; Dressler, R. A.; Berman, M. R. *J. Phys. Chem. A* **2000**, *104*, 10336.

(26) Lias, S. G.; Bartmess, J. E.; Liebman, J. F.; Holmes, J. L.; Levin, R. D.; Mallard, W. G. Ion Energetics Data. In *NIST Chemistry WebBook, NIST Standard Reference Database Number 69*; Mallard, W.G., Linstrom, P. J., Eds.; NIST: Gaithersburg, 1998; pp (http://webbook.nist.gov).

(27) Rebrion-Rowe, C.; Lehfaoui, L.; Rowe, B. R.; Mitchell, J. B. A. *J. Chem. Phys.* **1998**, *108*, 7185-7189.

(28) Abouelaziz, H.; Gomet, J. C.; Pasquerault, D.; Rowe, B. R.; Mitchell, J. B. A. *J. Chem. Phys.* **1993**, *99*, 237.

(29) Lehfaoui, L.; Rebrion—Rowe, C.; Laube, S.; Mitchell, J. B. A.; Rowe, B. R. *J. Chem. Phys.* **1997**, *106*, 5406-5412.

(30) Mitchell, J. B. A.; Rebrion-Rowe, C. *Int. Rev. Phys. Chem.* **1997**, *16*, 201-213.

(31) Mostefaoui, T.; Laube, S.; Gautier, G.; Rebrion-Rowe, C.; Rowe, B. R.; Mitchell, J. B. A. *J. Phys. B.: At. Mol. Opt. Phys.* **1999**, *32*, 5247.

(32) Viggiano, A. A.; Morris, R. A.; Dale, F.; Paulson, J. F.; Giles, K.; Smith, D.; Su, T. *J. Chem. Phys.* **1990**, *93*, 1149-1157.

(33) Miller, T. M.; Friedman, J. F.; Menendez-Barreto, M.; Viggiano, A. A.; Morris, R. A.; Miller, A.E. S.; Paulson, J. F. *Phys. Scripta* **1994**, *T53*, 84.

(34) Hierl, P. M.; Dotan, I.; Seeley, J. V.; Van Doren, J. M.; Morris, R. A.; Viggiano, A. A. *J. Chem. Phys.* **1997**, *106*, 3540-3544.

(35) Williams, S.; Knighton, W. B.; Midey, A. J.; Viggiano, A. A.; Irle, S.; Morikuma, K. *J. Phys. Chem. A* **2003**, Submitted.

(36) *NIST Chemistry WebBook, NIST Standard Reference Database No. 69*; Mallard, W. G.; Linstrom, P. J., Eds.; National Instututes of Standards and Technology: Gaithersburg, MD, 2001; Vol. (http://webbook.nist.gov/chemistry).

(37) Scott, G. B. I.; Fairley, D. A.; Milligan, D. B.; Freeman, C. G.; McEwan, M. J. *J. Phys. Chem. A* **1999**, *103*, 7470-7473.

(38) Smith, D.; Adams, N. G. *Int. J. Mass. Spectro. Ion Phys.* **1977**, *23*, 123.

(39) Adams, N. G.; Smith, D.; Lister, D. G.; Rakshit, A. B.; Tichy, M.; Twiddy, N. D. *Chem. Phys.Lett.* **1979**, *63*, 166-170.

(40) Williams, S.; Campos, M. F.; Midey, A. J.; Arnold, S. T.; Morris, R. A.; Viggiano, A. A. *J. Phys. Chem. A* **2002**, *106*, 997-1003.

(41) Koch, W.; Lin, B.; Schleyer, P. v. R. *J. Am. Chem. Soc.* **1989**, *111*, 3979.

(42) Lias, S. G.; Rebbert, R. E.; Ausloos, P. *J. Am.Chem. Soc.* **1970**, *92*, 6430-6440.

(43) Dymerski, P. P.; Prinstein, R. M.; Bente III, P.F.; McLafferty, F. W. *J. Am. Chem. Soc.* **1976**, *98*, 6834-6836.

(44) Attina, M.; Cacace, F.; Giacomello, P. *J. Am. Chem. Soc.* **1980**, *102*, 4768-4772.

(45) Shold, D. M.; P., A. *J. Am. Chem. Soc.* **1978**, *100*, 7915-7919.

(46) Meot-Ner (Mautner), M.; Field, F. H. *J. Am. Chem. Soc.* **1978**, *100*, 1356.

(47) Lossing, F. P.; Holmes, J. L. *J. Am. Chem. Soc.* **1984**, *106*, 6917-6920.

(48) Calcote, H. F.; Gill, R. J. *J. Phys. Chem. Ref. Data* **2002**, in press.

(49) Miller, T. M.; Doren, J. M. V.; Morris, R. A.; Viggiano, A. A. *Int. J. Mass Spectrom.* **2001**, *205*, 271.

(50) Nicolaides, A.; Rauk, A.; Glukhovtsev, M. N.; Radom, L. *J. Phys. Chem.* **1996**, *100*, 17460-17464.

(51) Leone, S.; Sontowski, J., Reentry Aerothermal Chemistry (REACH) Program User's Guide to the 3D Boundary Layer Code; Science Applications International Corporation: Fort Washington, PA, March 1991.

(52) Meot-Ner, M.; Field, F. H. *J. Phys. Chem.* **1976**, *80*, 2665.

(53) Meot-Ner, M.; Field, F. H. *J. Chem. Phys.* **1976**, *64*, 277.

(54) Ausloos, P.; Lias, S. G. *J. Am. Chem. Soc.* **1970**, *92*, 5037.

(55) Kalhori, S.; Viggiano, A. A.; Arnold, S. T.; Rosen, S.; Semaniak, J.; Derkatch, A. M.; Ugglas, M. a.; Larsson, M. *A&A* **2002**, *391*, 1159-1165.

(56) Pedersen, T.; Brown, R. C. *Comb. and Flame* **1993**, *94*, 433-448.